⌘ *Author's Choice*

THE JOURNAL OF BIOLOGICAL CHEMISTRY VOL. 283, NO. 30, pp. 20733–20744, July 25, 2008
© 2008 by The American Society for Biochemistry and Molecular Biology, Inc. Printed in the U.S.A.

Modulation of Voltage- and Ca^{2+}-dependent Gating of $Ca_V1.3$ L-type Calcium Channels by Alternative Splicing of a C-terminal Regulatory Domain*

Received for publication, March 21, 2008, and in revised form, May 13, 2008 Published, JBC Papers in Press, May 15, 2008, DOI 10.1074/jbc.M802254200

Anamika Singh[‡], Mathias Gebhart[‡], Reinhard Fritsch[§], Martina J. Sinnegger-Brauns[‡], Chiara Poggiani[‡], Jean-Charles Hoda[‡], Jutta Engel[¶], Christoph Romanin[§], Jörg Striessnig[‡], and Alexandra Koschak[‡1]

From the [‡]Institute of Pharmacy, Pharmacology, and Toxicology, and Center for Molecular Biosciences, University of Innsbruck, Peter-Mayr-Strasse 1/I, A-6020 Innsbruck, Austria, [§]Institute of Biophysics, University of Linz, Altenbergerstrasse 69, A-4040 Linz, Austria, and [¶]Institute of Physiology II and Tübingen Hearing Research Centre, University of Tübingen, D-72076 Tübingen, Germany

Low voltage activation of $Ca_V1.3$ L-type Ca^{2+} channels controls excitability in sensory cells and central neurons as well as sinoatrial node pacemaking. $Ca_V1.3$-mediated pacemaking determines neuronal vulnerability of dopaminergic striatal neurons affected in Parkinson disease. We have previously found that in $Ca_V1.4$ L-type Ca^{2+} channels, activation, voltage, and calcium-dependent inactivation are controlled by an intrinsic distal C-terminal modulator. Because alternative splicing in the $Ca_V1.3$ $\alpha1$ subunit C terminus gives rise to a long ($Ca_V1.3_{42}$) and a short form ($Ca_V1.3_{42A}$), we investigated if a C-terminal modulatory mechanism also controls $Ca_V1.3$ gating. The biophysical properties of both splice variants were compared after heterologous expression together with $\beta3$ and $\alpha2\delta1$ subunits in HEK-293 cells. Activation of calcium current through $Ca_V1.3_{42A}$ channels was more pronounced at negative voltages, and inactivation was faster because of enhanced calcium-dependent inactivation. By investigating several $Ca_V1.3$ channel truncations, we restricted the modulator activity to the last 116 amino acids of the C terminus. The resulting $Ca_V1.3_{\Delta C116}$ channels showed gating properties similar to $Ca_V1.3_{42A}$ that were reverted by co-expression of the corresponding C-terminal peptide C_{116}. Fluorescence resonance energy transfer experiments confirmed an intramolecular protein interaction in the C terminus of $Ca_V1.3$ channels that also modulates calmodulin binding. These experiments revealed a novel mechanism of channel modulation enabling cells to tightly control $Ca_V1.3$ channel activity by alternative splicing. The absence of the C-terminal modulator in short splice forms facilitates $Ca_V1.3$ channel activation at lower voltages expected to favor $Ca_V1.3$ activity at threshold voltages as required for modulation of neuronal firing behavior and sinoatrial node pacemaking.

Ca^{2+} influx through voltage-gated L-type Ca^{2+} channels (LTCCs)[2] regulates numerous physiological functions, including muscle contraction, hormone release, neuronal firing and plasticity, sensory function, and cardiac pacemaking (1). Four pore-forming $\alpha1$ subunit isoforms ($Ca_V1.1$–$Ca_V1.4$) with different biophysical properties and expression profiles evolved to adjust LTCC Ca^{2+} signals to cellular needs. $Ca_V1.3$ channels play a unique role for hearing (sensory signaling in cochlear inner hair cells (IHC)) and sinoatrial node (SAN, diastolic depolarization) function (2). $Ca_V1.3$ channels appear ideally suited for these functions because the operating range of both IHCs and SAN cells is within a voltage range of about −60 and −40 mV where these channels can conduct inward current because of their negative activation range (Refs. 3–5 and for review see Ref. 6). In neurons, $Ca_V1.3$ channels also serve pacemaker function and shape neuronal firing (7, 8). Ca^{2+} influx through LTCCs is limited by a Ca^{2+}-dependent feedback mechanism, the so-called calcium-dependent inactivation (CDI) (9). CDI develops in response to local or global elevations of intracellular Ca^{2+} sensed by channel-bound calmodulin (10, 11). However, moderation of CDI is an important prerequisite in some cells, such as in IHCs ($Ca_V1.3$; 12–14) and in retinal photoreceptors ($Ca_V1.4$), where slow inactivation of I_{Ca} is required for sensory signaling. In $Ca_V1.4$ channels, CDI is completely prevented by an intrinsic gating modulator located in the $Ca_V1.4\alpha1$ C terminus, and CDI is restored in C-terminal truncation mutants (15, 16). This C-terminal gating modulator (CTM) not only prevents CDI but also shifts the activation voltage range to more positive potentials (15). Gating modulation seems not to be limited to $Ca_V1.4$ because co-expression of C-terminal fragments of $Ca_V1.2$ channels also shifts their activation range to more positive voltages and inhibits pore opening (17). Because C termini of $Ca_V1.2$ (and also $Ca_V1.1$) $\alpha1$ subunits are proteolytically cleaved (18–20) but remain noncovalently bound to

* This work was supported by the Austrian Science Funds P17159 (to J. S.) and P18169 (to C. R.), the Tyrolean Science Fund UNI-0404/353 (to A. K.), European Community Grant Cavnet, MRTN-CT-2006-35367, and the University of Innsbruck. The costs of publication of this article were defrayed in part by the payment of page charges. This article must therefore be hereby marked "*advertisement*" in accordance with 18 U.S.C. Section 1734 solely to indicate this fact.

⌘ *Author's Choice*—Final version full access.

[2] The abbreviations used are: LTCC, L-type Ca^{2+} channel; ANOVA, analysis of variance; GFP, green fluorescent protein; YFP, yellow fluorescent protein; EYFP, enhanced YFP; CFP, cyan fluorescent protein; RT, reverse transcription; FRET, fluorescence resonance energy transfer; CTM, C-terminal gating modulator; CDI, calcium-dependent inactivation; DCRD, distal C-terminal regulatory domain; VDF, voltage-dependent facilitation; fwd, forward; rev, reverse; IHC, inner hair cells; GAPDH, glyceraldehyde-3-phosphate dehydrogenase; SAN, sinoatrial node; CaM, calmodulin; PCRD, primal C-terminal regulatory domain.

proximal C-terminal domains, they may serve as autoinhibitory modules (17, 21).

We hypothesized that $Ca_V1.3$ function may also be fine-tuned by a CTM domain similar to $Ca_V1.1$, $Ca_V1.2$, and $Ca_V1.4$. Unlike for other LTCC $\alpha1$ subunits, alternative splicing generates $Ca_V1.3$ $\alpha1$ subunits with long (usage of exon 42, $Ca_V1.3_{42}$) or short (usage of exon 42A, $Ca_V1.3_{42A}$) C termini. A CTM would therefore confer different biophysical properties on $Ca_V1.3$ only if present as in certain (*i.e.* long) variants.

Here we provide unequivocal evidence that an intramolecular protein-protein interaction gives rise to substantial gating differences between $Ca_V1.3_{42}$ and $Ca_V1.3_{42A}$. Our finding that the long and the short splice variants are expressed in several mouse and human tissues suggests that both contribute to fine-tuning of physiological $Ca_V1.3$ channel function.

EXPERIMENTAL PROCEDURES

Cloning of cDNA Constructs

To generate splice variant $Ca_V1.3_{42A}$, the alternatively spliced exon 42A was introduced into $Ca_V1.3$ cDNA ($Ca_V1.3_{42}$ = human $Ca_V1.3_{8A}$ as in Ref. 4, GenBank™ accession number EU363339) by co-ligating an EcoRI-BamHI-cut PCR product containing exon 42A from a rat brain $\alpha1$ subunit (GenBank™ accession number M57682) with HindIII-EcoRI-cut $Ca_V1.3$ cDNA into HindIII-BamHI (4622–7100)-cut $Ca_V1.3$-pBS vector. The rat exon 42A amino acid sequence is identical to its human homologue. Human $Ca_V1.3$ containing exon 42A was subsequently cloned into vector $pGFP^-$ (wild type) short form of the $Ca_V1.3$ protein (4). For analyzing the effects of exon 44, amino acid residues RTRYYETYI were introduced into an untagged construct containing the long $Ca_V1.3$ C terminus after position 1787 using standard PCR techniques. $Ca_V1.3_{\Delta C473}$, $Ca_V1.3_{\Delta C158}$, $Ca_V1.3_{\Delta C116}$, and $Ca_V1.3_{\Delta C76}$ channels were constructed by introducing stop codons into untagged $Ca_V1.3_{42}$ at respective amino acid positions 1665, 1980, 2022, and 2062 followed by artificial restriction sites as follows: BamHI* for $Ca_V1.3_{\Delta C158}$ and $Ca_V1.3_{\Delta C76}$, HpaI* for $Ca_V1.3_{\Delta C116}$, and XhoI* for $Ca_V1.3_{\Delta C473}$. Peptides GFP-C_{158}, GFP-C_{116}, and GFP-C_{76} were constructed by ligating HindIII*-SalI*-flanked PCR products corresponding to amino acids 1980–2137, 2022–2137, and 2062–2137 of $Ca_V1.3_{42}$ into the $pGFP^+$ plasmid resulting in the corresponding GFP-tagged $Ca_V1.3$ C-terminal peptides (22). For FRET analysis, all C-terminal $Ca_V1.3$ fragments were cloned either into the mammalian expression vector *pEYFP-C1* for N-terminal EYFP labeling or vector *pECFP-N1* for C-terminal enhanced CFP labeling (Clontech). N-terminally EYFP-labeled constructs 5′-HindIII* and 3′-SalI* restriction sites flanking nucleotide sequences corresponding to the following $Ca_V1.3$ amino acid positions were introduced and cloned into HindIII-SalI-cut vector *pEYFP-C1* as follows: peptide EF-preIQ-IQ-postIQ, amino acids 1453–2137; EF-preIQ-IQ, amino acids 1453–1623; and EF-preIQ-IQ-PCRD, amino acids 1453–1664. To construct peptide EF-preIQ-IQ-$PCRD^{RRQQ}$, arginines at positions 1640 and 1641 were mutated to glutamines by splicing by overlapping extension-PCR. For C_{158}-CFP and C_{116}-CFP, 5′-EcoRI* and 3′-BamHI* restriction sites were introduced to flanking nucleotide sequences corresponding to $Ca_V1.3$ amino acid positions 1980–2137 and 2022–2137 and cloned into EcoRI-BamHI-cut vector *pECFP-N1*. To generate enhanced CFP-C_{116}^{DEQQ}, aspartate and glutamate at positions 2073 and 2076 were mutated to glutamines by splicing by overlapping extension-PCR. Integrity of all constructs was confirmed by DNA sequencing (MWG Biotec, Martinsried, Germany). Construct $Ca_V1.3_{42}$ was subjected to full-length sequence analysis. Numbering of amino acids or nucleotide positions in all constructs refers to GenBank™ accession number EU363339. Asterisks indicate artificial restriction sites introduced by PCR.

Qualitative RT-PCR

Mouse tissue was prepared from C57B/6N wild-type mice. Total RNA was isolated from whole-brain and brain sub-regions using the RNAqueos®-4PCR kit (Ambion, Foster City, CA). After DNase I treatment, RNA integrity was checked by the quality of the 28 S and 18 S rRNA bands on a denaturing agarose gel. Organ of Corti mRNA was prepared from P4 or P19 mice as described in Ref. 23. Human total RNAs from brain, heart, pancreas, and retina were purchased from Clontech. One μg of total RNA was used for first strand cDNA synthesis by reverse transcriptase (RevertAid™ H Minus First Strand cDNA synthesis kit, MBI; Fermentas, Hanover, Germany) and random hexamer primers. For PCR analysis, the forward (fwd) primer was located in exon 39 (GenBank™ accession number NM_028981 for mouse and EU363339 for human). To differentiate between $Ca_V1.3_{42}$ and $Ca_V1.3_{42A}$, specific reverse (rev) primers were designed, located either in exon 42 or 42A. The following primers were used for mouse: fwd primer, 5′-CAACCCTGTTTGCTTTGGTC-3′, and rev primer for exon 42, 5′-TATAGCCCGTCGGATTTCTG-3′ (332-bp product); rev primer for exon 42A, 5′-CTTCCTTCCGGAGGAGTGC-3′ (483-bp product). The following primers were used for human: fwd primer, 5′-AACCCTGTTTGCTTTGGTTC-3′, rev primer for exon 42, 5′-TATAGCACGCCGGATTTCTG-3′ (331-bp product); rev primer for exon 42A, 5′-CCACCTTCCGGAGGAGTG-3′ (488-bp product). In mouse organ of Corti, splice variants were also detected with the following primer pairs: exon 42 fwd primer, 5′-CTGCTTGACCAAGTTGTCCCTCCA-3′, rev primer, 5′-CTACAAGGTGGTAATGCAAATCAT-3′; exon 42A, fwd primer, 5′-CGCGGATCCTACTTGACCAAGTTGTCCC-3′; rev primer, 5′-CGCAAGCTTCTAGAGCATCCGTTCAAGC-3′. Mouse and human GAPDH was used as positive control as follows: for mouse (GenBank™ accession number NM_008084), fwd primer, 5′-ACTCCACTCACGGCAAATTC-3′, rev primer 5′-CACATTGGGGGTAGGAACAC-3′ (572-bp product); for human (GenBank™ accession number NM_002046), fwd primer, CAATGACCCCTTCATTGACC, rev primer, 5′-GAGGCAGGGATGATGTTCTG-3′ (531-bp product). 500 ng (2.7 μg for organ of Corti) of reverse-transcribed cDNA was used as template for each PCR. Samples without template were used as contamination control. The following PCR program was used: 94 °C for 3 min, 40 cycles of 94 °C for 45 s, 55 °C for 45 s, and 68 °C for 1 min, followed by an elongation step of 68 °C for 10 min. PCRs were performed using BioTherm™ TaqDNA polymerase (GeneCraft, Lüdinghausen, Germany) in the presence

of 1.5 mM $MgCl_2$. The resulting PCR products were subcloned into pGEM-T Easy vectors (Promega, Mannheim, Germany) and sequenced.

Quantitative RT-PCR

RNA Isolation and cDNA Preparation—Tissue from three adult male c57BL/6N mice (3–6 months) was used for whole-brain and brain sub-region cDNA preparations. Total RNA and cDNA were prepared as described (24).

Quantitative RT-PCR—The relative abundance of different $Ca_V1.3$ mRNAs was assessed by TaqMan quantitative PCR (50 cycles) using a standard curve method as described (24). TaqMan gene expression assays, designed to span exon-exon boundaries, were purchased from Applied Biosystems (Foster City, CA). Assessment of mouse GAPDH transcripts was included as efficiency reference. Assay identification numbers are as follows: exon 42, Mm0551393_m1 (efficiency (E) = 103.6%); exon 42A (E = 98.7%), custom-designed (fwd primer, 5′-GGAAGTACCCTGCGAAGAACAC-3′; probe, 5′-TTGCCCTACAGATGCTTG-3′; rev primer, 5′-CTCAGGCAGAGAACTCTAAAGCAT-3′); GAPDH, Mm99999915_g1. To amplify specific cDNA templates from the analyzed tissues for the standard curves of each assay, primer pairs were as follows: exon 42 fwd primer, 5′-CAACCCTGTTTGCTTTGGTC-3′, rev primer, 5′-TGATTGACATGGTTTCCAAGC-3′; exon 42A fwd primer, 5′-CAACCCTGTTTGCTTTGGTC-3′, rev primer, 5′-CTTCCTTCCGGAGGAGTGC-3′. Analysis was carried out in triplicate.

Cell Culture and Transient Expression—HEK-293 (tsA-201) cells were cultured and transfected as described previously (4). Untagged $Ca_V1.3\alpha1$ constructs were expressed together with $\beta3$ (or $\beta2a$) and $\alpha_2\delta$ 1 subunits (4). In co-expression studies, GFP-labeled C-terminal $Ca_V1.3$ fragments were used to ensure the presence of the corresponding C-terminal peptide in the cell recorded. Immunoblotting was performed as described previously (25) using a generic anti-$\alpha1$ sequence-directed antibody as described previously (4). All constructs were expressed with the expected molecular mass.

Electrophysiological Recordings—Whole-cell patch clamp recordings in transiently transfected HEK-293 (tsA-201) cells were performed 2–3 days after transfection using either 15 mM Ba^{2+} or Ca^{2+} as charge carrier as described in Ref. 4. Recording solutions were composed as follows (in mM): intracellular solution, 135 CsCl, 10 Cs-EGTA, 1 $MgCl_2$ adjusted to pH 7.4 with CsOH (311 mosM); bath solution, 15 $BaCl_2$, 10 HEPES, 150 choline-Cl, and 1 $MgCl_2$, adjusted to pH 7.4 with CsOH (358 mosM). Transfected cells were visualized by co-expression of GFP or GFP- or YFP-labeled constructs co-expressed with the channel complex as indicated. Current-voltage (I-V) relationships were obtained by holding cells at a potential of −90 mV before applying 50-ms or 300-ms pulses to various test potentials. I-V curves were fitted to the equation $I = G_{max}(V - V_{rev})/\{1 + \exp((V - V_{0.5act})/k)\}$, where V_{rev} is the extrapolated reversal potential; V is the test potential; I is the peak current amplitude; G_{max} is the maximum slope conductance; $V_{0.5,act}$ is the half-maximal activation voltage; and k is the slope factor. Percentage of inactivation was determined at specified time points during depolarizing pulses from a holding potential of −90 mV to the peak current potential (V_{max}) of the I–V relation of the individual cell. The voltage dependence of inactivation was assessed by application of a 20-ms test pulse to V_{max} before and after holding cells at various conditioning test potentials for 5 s. Steady-state inactivation curves were analyzed using the Boltzmann relationship $I = I_{SS} + (1 - I_{SS})/(1 + \exp(V - V_{0.5,inact}/k_{inact}))$, where I is the peak current amplitude; I_{SS} is the noninactivating fraction; V is the membrane potential; $V_{0.5,inact}$ is the half-inactivation potential; and k_{inact} is the slope factor. To investigate $Ca_V1.3_{42}$ and $Ca_V1.3_{42A}$ gating properties, head-to-head analysis was performed time-independently by two investigators. Experiments showing currents bigger than 3 nA were prospectively excluded from analysis of activation and inactivation parameters to guarantee high quality voltage clamp. CDI was quantified as the current remaining at the end of 250-ms depolarizations to different test potentials, expressed as fraction of peak current amplitude (r_{250}). Parameter f was defined as the difference between r_{250} values of I_{Ba} and I_{Ca} at +10 mV. CDI experiments were performed on different cells, but effects were the same when the charge carrier was switched from Ba^{2+} to Ca^{2+} on the same cell in representative experiments. All voltages were corrected for the liquid junction potential.

Confocal FRET Microscopy

Confocal FRET microscopy was performed as described previously (15). As negative controls, peptide *YFP*-EF-PreIQ-IQ-PCRD was co-expressed with CFP alone (CFP control), and probes *CFP*-C_{158} or *CFP*-C_{116} with YFP alone (YFP controls 1 and 2). Image analysis was accomplished using a self-made program integrated in MatLab 7 based on the FRET analysis algorithm proposed (26). Interaction between fragments was considered when a significant difference to the CFP as well as the corresponding YFP control was observed. The local ratio between CFP and YFP might vary because of different local expression levels of the different protein constructs, which could affect calculation of FRET values. Therefore, analysis was limited to pixels with a CFP:YFP molar ratio between 1:10 and 10:1.

Statistical Analysis

Data were analyzed using Clampfit® 9.0 (Molecular Devices, Union City, CA) and Microcal Origin® 5.0 (Northampton, MA). Significant difference between the two splice variants was assessed *a priori* by pairwise comparison before other truncation constructs to characterize the modulatory mechanism were made. Student's t test or Mann-Whitney test were used for comparison between two groups for parametric and nonparametric data, respectively. Statistical significance was determined using one-way ANOVA followed by Bonferroni post-test, except if stated otherwise. Statistical significance was set at $p < 0.05$. All data are presented as mean ± S.E. for the indicated number of experiments.

RESULTS

$Ca_V1.3$ C-terminal Modulator Affects Voltage-dependent Channel Activity—To test for the presence of a C-terminal modulator (CTM), we employed two previously described nat-

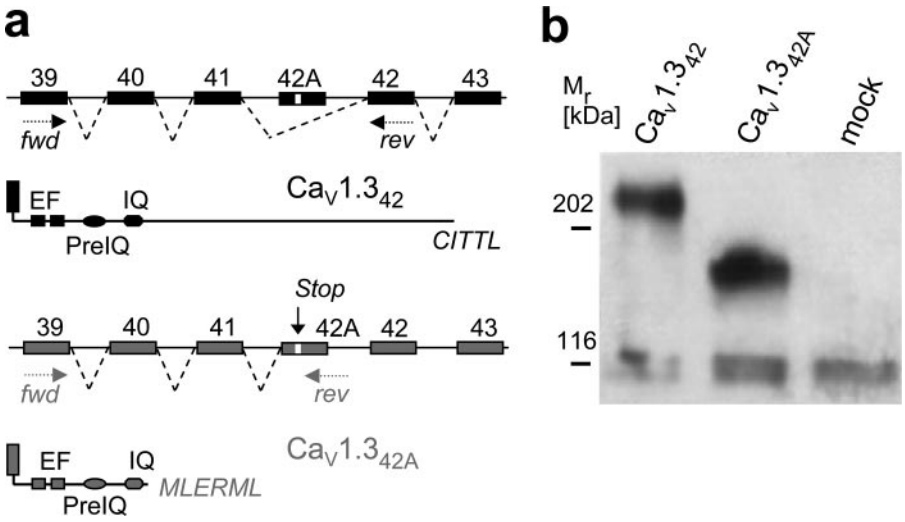

FIGURE 1. **C-terminal splice variants $Ca_V1.3_{42}$ and $Ca_V1.3_{42A}$.** *a,* alternative usage of exon 42 results in either full-length (exon 42, *black*) or C-terminally truncated (exon 42A, *gray*) $Ca_V1.3$ channels. *Arrows* indicate the approximate position of forward (*fwd*) and reverse (*rev*) PCR primers used in Fig. 8. *b,* immunoblot of both splice variants expressed together with $\beta3$ and $\alpha2\delta1$ subunits in HEK-293 cells, as described under "Experimental Procedures." Mock-transfected cells (*mock*) were used to show specificity of immunoreactivity. One representative experiment out of four is shown.

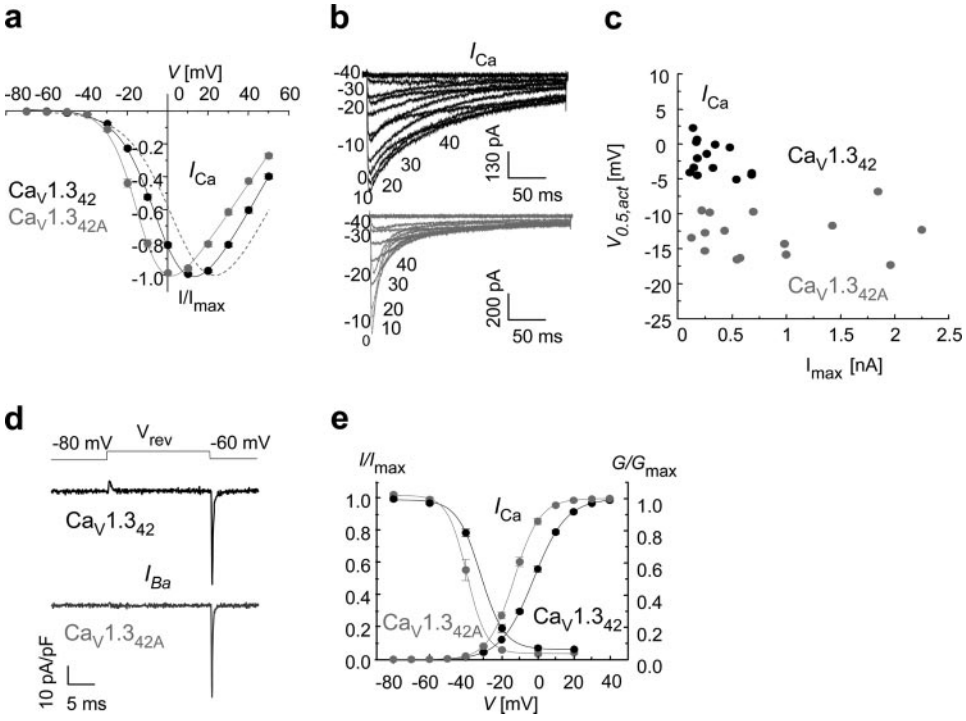

FIGURE 2. **Activation and steady-state inactivation properties of $Ca_V1.3_{42}$ compared with $Ca_V1.3_{42A}$ channels.** *a,* normalized mean *I-V* curves of I_{Ca} for $Ca_V1.3_{42}$ (*black*) and $Ca_V1.3_{42A}$ (*gray*) channels. Activation parameters and statistics are given in Table 1. The *dotted line* describes the fit to a normalized *I-V* curve of I_{Ca} for $Ca_V1.2$ in comparison: $V_{0.5,act}$, 8.8 mV; k_{act}, −11.0 mV. Cell, 111d_16. *b,* representative current traces for I_{Ca} (300-ms depolarization to indicated test potentials). Cells: $Ca_V1.3_{42}$, 196l_23; $Ca_V1.3_{42A}$, 196l_32. *c,* $V_{0.5,act}$ for $Ca_V1.3_{42A}$ was independent from current density. *d,* exemplar ON-gating currents for $Ca_V1.3_{42}$ and $Ca_V1.3_{42A}$ with similar I_{Ba} amplitudes measured by depolarizing cells to V_{rev}. One representative out of six experiments is shown. Cells: $Ca_V1.3_{42}$, 207l_34; $Ca_V1.3_{42A}$, 237k_26. *e,* steady-state inactivation curves for $Ca_V1.3_{42}$ and $Ca_V1.3_{42A}$. Activation curves were obtained from parameters in *a*. *Solid lines* are fits to the Boltzmann relationship (see "Experimental Procedures"). Statistics are given under "Results." *Error bars* reflect S.E.

urally occurring $Ca_V1.3$ $\alpha1$ subunit splice variants, $Ca_V1.3_{42}$ and $Ca_V1.3_{42A}$ (also termed $Ca_V1.3a$ and $Ca_V1.3b$, respectively (5, 27, 28)), which differ with respect to the length of their C termini, as illustrated in Fig. 1*a*. Similar to the $Ca_V1.4$ truncation mutant K1591*X* (15), $Ca_V1.3_{42A}$ terminates shortly after the IQ motif and lacks most of a homologous region (termed PCRD) previously found to participate in the binding of distal C-terminal sequences in $Ca_V1.2$ (17). Wild-type long and short $Ca_V1.3$ $\alpha1$ subunits were expressed in HEK-293 cells together with $\beta3$ (or $\beta2a$) and $\alpha2\delta1$. $\beta3$ subunits were selected because we have previously shown that they form a large fraction of dihydropyridine-sensitive LTCCs in the brain (29). Both $\alpha1$ subunits migrated with the expected molecular mass in Western blots of HEK-293 cell preparations (Fig. 1*b*).

We systematically investigated the biophysical properties of both I_{Ca} and I_{Ba} for $Ca_V1.3_{42}$ and $Ca_V1.3_{42A}$ as illustrated in Figs. 2 and 3 and Tables 1–3. The voltage dependence of I_{Ca} activation of $Ca_V1.3_{42A}$ was significantly shifted to hyperpolarizing potentials by about 10 mV ($Ca_V1.3_{42}$: $V_{0.5,act} = -2.2 \pm 0.6$ mV, $n = 14$; $Ca_V1.3_{42A}$: $V_{0.5,act} = -12.9 \pm 0.8$ mV, $n = 15$; $p < 0.001$; see Table 1). This negative shift was because of the significant decrease in k_{act} ($Ca_V1.3_{42}$: -9.1 ± 0.2, $n = 14$; $Ca_V1.3_{42A}$: -6.9 ± 0.2, $n = 15$; $p < 0.001$; see Table 1) without change in the activation threshold (Fig. 2*a*). Such changes were also observed for I_{Ba} (Table 2). The negative activation range persisted when subgroups of cells with different current amplitudes (0.1–0.6 *versus* 0.7–2.3 nA) were compared (Fig. 2*c*). It was not restricted to $\beta3$ subunit-containing channel complexes because it was also seen when the $Ca_V1.3$ splice variants were co-expressed with $\beta2a$ subunits ($V_{0.5,act}$, I_{Ca}, $Ca_V1.3_{42}$, $V_{0.5,act}$, 0.06 ± 3.2 mV, $n = 3$, $Ca_V1.3_{42A}$, $V_{0.5,act}$, -11.2 ± 1.7 mV, $n = 3$; I_{Ba}, $Ca_V1.3_{42}$, -12.5 ± 1.6 mV, $n = 7$, $Ca_V1.3_{42A}$, -22.7 ± 1.3 mV, $n = 6$). Mean current density of $Ca_V1.3_{42A}$ channels was ~2.5-fold higher for I_{Ca} ($Ca_V1.3_{42}$, 21.0 ± 3.3 pA/pF, $n = 14$; $Ca_V1.3_{42A}$, 98.3 ± 31.8, $n = 19$, $p < 0.01$, Mann-Whitney test). A similar increase was observed for I_{Ba} (not shown). Increased current density occurred without detectable changes in the expression density as observed in immunoblots

TABLE 1

Biophysical I_{Ca} properties of $Ca_V1.3_{42}$ and $Ca_V1.3_{42A}$ channels in comparison with different C-terminally truncated $Ca_V1.3$ channel constructs

Number of experiments is indicated in parentheses.

Construct	$V_{0.5,act}$	k_{act}	V_{max}	Activation threshold	V_{rev}
	mV	*mV*	*mV*	*mV*	*mV*
$Ca_V1.3_{42}$ (14)	−2.2 ± 0.6[a]	−9.1 ± 0.2[a]	13.3 ± 0.6[a]	−35.6 ± 0.7	69.8 ± 1.1
$Ca_V1.3_{42A}$ (15)	−12.9 ± 0.8[b]	−6.9 ± 0.2[b]	1.9 ± 0.9[b]	−37.1 ± 0.8	65.7 ± 1.1
$Ca_V1.3_{\Delta C158}$ (9)	−14.3 ± 0.4[b]	−7.4 ± 0.2[b]	0.7 ± 0.5[b]	−38.9 ± 0.6[c]	62.4 ± 1.3[b]
$Ca_V1.3_{\Delta C116}$ (10)	−12.0 ± 0.7[b]	−7.7 ± 0.3[d]	3.0 ± 0.8[b]	−38.4 ± 0.5	61.4 ± 1.1[b]
$Ca_V1.3_{\Delta C76}$ (12)	−14.6 ± 0.9[b]	−7.0 ± 0.3[b]	0.8 ± 1.2[b]	−38.1 ± 0.4	63.5 ± 1.3[d]
$Ca_V1.3_{\Delta C473}$ (9)	−12.8 ± 1.4[b]	−7.3 ± 0.4[b]	2.1 ± 1.7[b]	−37.1 ± 1.1	64.7 ± 1.3
$Ca_V1.3_{42A} + C_{158}$ (7)	−12.6 ± 1.5[b]	−7.6 ± 0.3[d]	2.8 ± 1.5[b]	−38.9 ± 0.7	63.6 ± 2.2[c]
$Ca_V1.3_{\Delta C158} + C_{158}$ (8)	−0.8 ± 1.4[a]	−9.7 ± 0.4[a]	13.9 ± 1.2[a]	−36.5 ± 0.9	67.5 ± 1.2
$Ca_V1.3_{\Delta C116} + C_{116}$ (7)	−4.2 ± 0.7[a]	−9.1 ± 0.4[a]	10.0 ± 0.6[a]	−38.2 ± 0.9	61.5 ± 1.3[b]
$Ca_V1.3_{\Delta C76} + C_{76}$ (11)	−13.8 ± 0.9[b]	−7.1 ± 0.2[b]	1.5 ± 1.2[b]	−37.2 ± 0.7	61.5 ± 1.3[b]
$Ca_V1.3_{\Delta C473} + C_{116}$ (9)	−3.1 ± 1.4[a]	−9.1 ± 0.3[a]	11.7 ± 1.2[a]	−35.7 ± 0.3	65.4 ± 0.9

[a] For statistics, $p < 0.001$ compared with $Ca_V1.3_{42A}$ (one-way ANOVA followed by Bonferroni post-test).
[b] Values are $p < 0.001$ (statistically significant from $Ca_V1.3_{42}$).
[c] Values are $p < 0.05$.
[d] Values are $p < 0.01$.

TABLE 2

Biophysical I_{Ba} properties of $Ca_V1.3_{42}$ and $Ca_V1.3_{42A}$ channels in comparison with different C-terminally truncated $Ca_V1.3$ channel constructs

Number of experiments is indicated in parentheses.

Construct	$V_{0.5,act}$	k_{act}	V_{max}	Activation threshold	V_{rev}
	mV	*mV*	*mV*	*mV*	*mV*
$Ca_V1.3_{42}$ (18)	−11.8 ± 0.9[a]	−7.8 ± 0.2[b]	3.4 ± 0.9[b]	−39.9 ± 0.7[b]	58.2 ± 0.9[a]
$Ca_V1.3_{42A}$ (12)	−20.2 ± 1.0[c]	−6.6 ± 0.3[d]	−6.6 ± 1.2[d]	−43.3 ± 0.6[d]	50.7 ± 1.6[c]
$Ca_V1.3_{\Delta C158}$ (12)	−20.9 ± 1.2[c]	−5.7 ± 0.3[c]	−8.4 ± 1.5[c]	−41.7 ± 0.5	46.4 ± 1.6[c]
$Ca_V1.3_{\Delta C116}$ (9)	−22.9 ± 0.6[c]	−5.9 ± 0.2[c]	−10.3 ± 0.8[c]	−43.7 ± 0.5[d]	44.2 ± 1.2[c,e]
$Ca_V1.3_{\Delta C76}$ (10)	−22.8 ± 0.5[c]	−5.5 ± 0.1[c]	−9.9 ± 0.6[c]	−41.9 ± 0.4	48.1 ± 0.8[c]
$Ca_V1.3_{\Delta C473}$ (6)	−22.2 ± 0.9[c]	−5.9 ± 0.1[c]	−8.9 ± 1.0[d]	−42.2 ± 0.7	49.1 ± 0.7[c]
$Ca_V1.3_{42A} + C_{158}$ (7)	−22.2 ± 1.2[c]	−6.1 ± 0.4[c]	−8.8 ± 1.5[c]	−44.1 ± 0.9[c]	48.8 ± 1.1[c]
$Ca_V1.3_{\Delta C158} + C_{158}$ (11)	−10.3 ± 0.9[a]	−8.2 ± 0.2[a]	3.6 ± 0.8[a]	−40.1 ± 0.7[e]	56.4 ± 1.2[e]
$Ca_V1.3_{\Delta C116} + C_{116}$ (7)	−13.3 ± 1.2[a]	−7.8 ± 0.2[e]	1.2 ± 1.2	−41.2 ± 0.9	54.9 ± 1.3
$Ca_V1.3_{\Delta C76} + C_{76}$ (9)	−22.1 ± 0.8[c]	−5.9 ± 0.2[c]	−7.5 ± 1.3[c]	−42.6 ± 0.6	49.2 ± 1.2[c]
$Ca_V1.3_{\Delta C473} + C_{116}$ (11)	−15.6 ± 1.2[e]	−7.6 ± 0.1[e]	−1.7 ± 1.1[d,e]	−42.9 ± 0.8[d]	50.8 ± 0.8[c]

[a] For statistics, $p < 0.001$ compared with $Ca_V1.3_{42A}$ (for multiple comparison test, see Table 1).
[b] Values are $p < 0.01$.
[c] Values are $p < 0.001$ (statistically significant from $Ca_V1.3_{42}$).
[d] Values are $p < 0.01$.
[e] Values are $p < 0.05$.

(Fig. 1*b*, $n = 4$). Depolarization to the reversal potential (V_{rev}) revealed a small ON-gating current which was always detectable for $Ca_V1.3_{42}$ channels but was absent (or much reduced) in $Ca_V1.3_{42A}$ currents (Fig. 2*d*). This further suggests that the larger current amplitude of $Ca_V1.3_{42A}$ channels was not because of an increased expression density of channels at the plasma membrane in line with the immunoblot analysis.

The short C terminus also resulted in a slight decrease of V_{rev} (with a larger and statistically significantly difference for I_{Ba}; see Tables 1 and 2). The half-maximal voltage of steady-state inactivation ($V_{0.5,inact}$) induced by 10-s conditioning pulses (Fig. 2*e*) for the physiological charge carrier was also significantly shifted toward more negative voltages in $Ca_V1.3_{42A}$ channels ($Ca_V1.3_{42}$: −31.6 ± 1.1 mV, $n = 5$; $Ca_V1.3_{42A}$: −38.8 ± 1.6 mV, $n = 4$, $p = 0.007$, Student's *t* test). A significant difference in the slope factor (k_{inact}, $Ca_V1.3_{42}$: −6.4 ± 0.3 mV, $n = 5$; $Ca_V1.3_{42A}$: −4.9 ± 0.5 mV, $n = 4$, $p = 0.03$, Student's *t* test) was also observed. Theses changes in the voltage dependence of steady-state activation and inactivation resulted in a shift of the window current toward more hyperpolarizing voltages for $Ca_V1.3_{42A}$ (Fig. 2*e*). Our data demonstrate that the structural divergence within the C termini of these $Ca_V1.3$ splice variants causes pronounced changes in channel gating suggesting the existence of a CTM in $Ca_V1.3$ LTCCs that controls their activity at negative voltages.

$Ca_V1.3$ C Terminus Modulates Ca^{2+}-dependent Inactivation Properties—As already obvious from the representative current traces in Fig. 2*b*, $Ca_V1.3_{42A}$ channels inactivate faster during depolarization to different test potentials than $Ca_V1.3_{42}$ channels. This is also evident from a detailed comparison of I_{Ca} inactivation during 10-s pulses to the maximum of the *I-V* curve (V_{max}) (Fig. 3, *a* and *b*; Table 3). The difference was most pronounced during the first 30 ms (% inactivation: $Ca_V1.3_{42}$, 27.5 ± 1.9, $n = 16$; $Ca_V1.3_{42A}$, 73.6 ± 1.9, $n = 19$, $p < 0.001$; Fig. 3, *a*, *inset*, and *b*, and Table 3). Inactivation included an initial fast component followed by a slow component in both isoforms. Inactivation was not complete even during 10 s ($Ca_V1.3_{42}$, 96.9 ± 0.7%, $n = 14$; $Ca_V1.3_{42A}$, 98.1 ± 0.3%, $n = 17$; one sample *t* test, compared with 100%: $p = 0.0006$ for $Ca_V1.3_{42}$ and $p = 0.0001$ for $Ca_V1.3_{42A}$) suggesting that some Ca^{2+} influx through $Ca_V1.3$ channels may persist even during extended periods of strong depolarization. Faster I_{Ca} inactivation of $Ca_V1.3_{42A}$ was also seen at physiologically more relevant potentials, as indicated by a significant decrease in integrated I_{Ca} during 300-ms test pulses (Fig. 3*c*). Note that voltage dependence of activation and inactivation is shifted by ~15 mV to more positive voltages under our recording conditions (5). Therefore, −20 mV corresponds to about −35 mV at physiological Ca^{2+} concentrations.

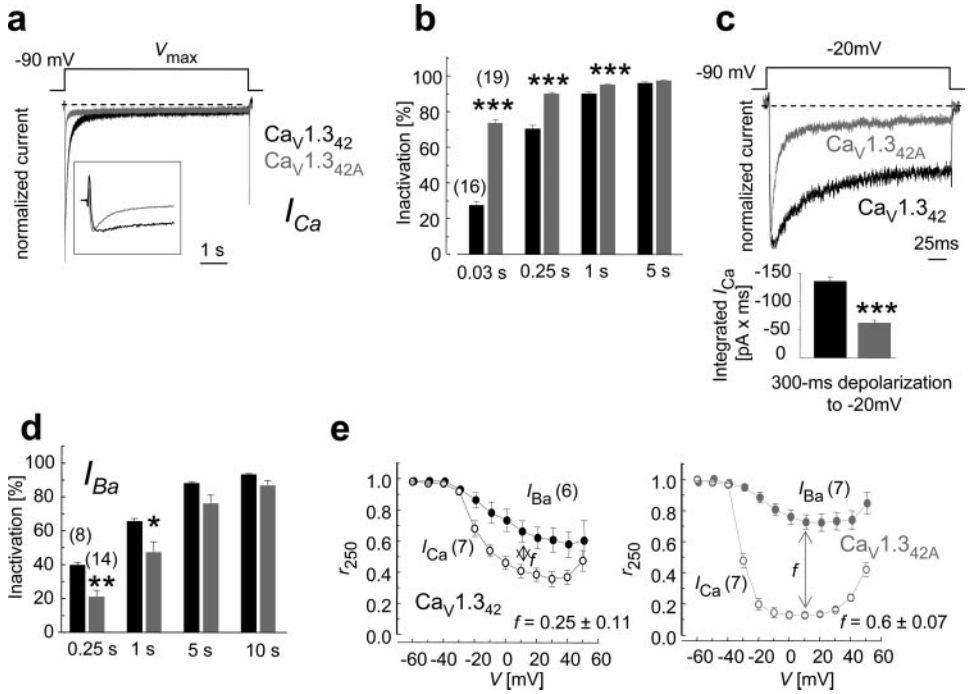

FIGURE 3. **Inactivation properties of $Ca_V1.3_{42}$ and $Ca_V1.3_{42A}$ channel-mediated currents.** *a*, representative current traces of $Ca_V1.3_{42}$ (*black*) and $Ca_V1.3_{42A}$ (*gray*) I_{Ca} evoked by a 10-s depolarization to V_{max}. The *inset* illustrates inactivation during initial 30 ms. Cells: $Ca_V1.3_{42}$, 316h_51; $Ca_V1.3_{42A}$, 187g_46. *b*, percent I_{Ca} inactivation during 0.03-, 0.25-, 1-, and 5-s test pulses to V_{max}. ***, $p \leq 0.001$, Student's *t* test. *c*, normalized representative I_{Ca} traces at physiologically relevant potentials (−20 mV; corresponding to ~−35 mV at physiological Ca^{2+} concentrations; see "Results"). Cells: $Ca_V1.3_{42}$, 196l_23; $Ca_V1.3_{42A}$,187g_17. Integrated current corresponding to the area under normalized I_{Ca} during a 300-ms pulse is shown. Statistically significant difference: ***, $p \leq 0.001$, Unpaired *t* test. *d*, percent I_{Ba} inactivation during 0.03-, 0.25-, 1-, and 5-s test pulses to V_{max}. *, $p < 0.05$; **, $p < 0.01$, Student *t* test. *e*, voltage dependence of CDI for $Ca_V1.3_{42}$ (*left*) and $Ca_V1.3_{42A}$ (*right*): r_{250} corresponds to the fraction of I_{Ca} or I_{Ba} remaining after 250 ms; *f* is the difference between r_{250} values at +10 mV (for statistics see "Results" and Table 3). Number of experiments is given in parentheses. *Error bars* reflect S.E.

TABLE 3

I_{Ca} and I_{Ba} inactivation and CDI properties of $Ca_V1.3_{42}$ and $Ca_V1.3_{42A}$ channels in comparison with different C-terminally truncated $Ca_V1.3$ channel constructs

Number of experiments is indicated in parentheses.

Construct	I_{Ca} inactivation during 30 ms	I_{Ba} inactivation during 250 ms	*f* value, $n = 6–11$
	%	%	
$Ca_V1.3_{42}$	27.5 ± 1.9[a] (16)	39.8 ± 1.6[a] (8)	0.25 ± 0.11
$Ca_V1.3_{42A}$	73.6 ± 1.9[b] (19)	21.1 ± 3.8[b] (14)	0.60 ± 0.07
$Ca_V1.3_{\Delta C158}$	70.4 ± 2.2[b] (8)	16.9 ± 3.5[b] (7)	0.60 ± 0.05
$Ca_V1.3_{\Delta C116}$	72.6 ± 1.5[b] (8)	8.5 ± 1.9[b,c] (9)	0.66 ± 0.05
$Ca_V1.3_{\Delta C76}$	74.3 ± 1.8[b] (9)	14.9 ± 1.9[b] (11)	0.72 ± 0.04
$Ca_V1.3_{\Delta C473}$	71.7 ± 1.3[b] (7)	15.9 ± 2.9[b] (8)	0.67 ± 0.06
$Ca_V1.3_{42A} + C_{158}$	67.1 ± 2.5[b] (6)	10.3 ± 1.3[b] (5)	0.71 ± 0.06
$Ca_V1.3_{\Delta C158} + C_{158}$	23.5 ± 1.9[a] (8)	30.2 ± 2.5 (12)	0.20 ± 0.08
$Ca_V1.3_{\Delta C116} + C_{116}$	34.8 ± 2.0[c] (7)	35.3 ± 2.7[c] (7)	0.29 ± 0.05
$Ca_V1.3_{\Delta C76} + C_{76}$	67.2 ± 2.4[b] (7)	18.5 ± 2.6[b] (9)	0.56 ± 0.06
$Ca_V1.3_{\Delta C473} + C_{116}$	32.2 ± 4.6[a] (8)	35.4 ± 1.9[c] (9)	0.27 ± 0.05

[a] For statistics, $p < 0.001$ compared with $Ca_V1.3_{42A}$ (for multiple comparison test, see Table 1).
[b] Values are $p < 0.001$ (statistically significant from $Ca_V1.3_{42}$).
[c] Values are $p < 0.01$.

The faster inactivation of $Ca_V1.3_{42A}$ could be due to faster voltage-dependent inactivation, faster CDI, or both. To address this question, we also quantified $Ca_V1.3$-mediated I_{Ba} of both splice variants. Interestingly, mean I_{Ba} inactivation was even slower for $Ca_V1.3_{42A}$ channels (Fig. 3*d* and Table 3). This difference was because of a pronounced slowing of inactivation in 50% of the cells (% inactivation of $Ca_V1.3_{42A}$ during 250 ms, 8.6 ± 1.2%, $n = 7$, in this subset). We have previously observed a similar slowing of inactivation of I_{Ba} in truncated $Ca_V1.4$ channels (15).

From these data we conclude that the faster inactivation of I_{Ca} observed for $Ca_V1.3_{42A}$ must be due to more pronounced CDI. As a quantitative measure of CDI, we analyzed the fraction of I_{Ca} through $Ca_V1.3$ channels remaining after a 250-ms depolarization (r_{250}) in a wide voltage range (Fig. 3*e*). A typical U-shaped dependence on test voltage was observed for both splice variants, but it was more pronounced for $Ca_V1.3_{42A}$ channels ($f = 0.60 \pm 0.07$ *versus* 0.25 ± 0.11 at 10 mV for $Ca_V1.3_{42}$ channels). In agreement with a previous report (13), $Ca_V1.3$ CDI was CaM-mediated. I_{Ca} inactivation of $Ca_V1.3_{42A}$ channels was dramatically slowed by co-expression of YFP-labeled dominant-negative CaM (CaM_{1234}) (r_{250} at V_{max}: $Ca_V1.3_{42A} + CaM_{1234}$, 0.76 ± 0.061%, $n = 5$, $p < 0.0001$, Student's *t* test *versus* $Ca_V1.3_{42A}$) thus approaching r_{250} values for I_{Ba} (for comparison see Fig. 3*e*). CaM_{1234} did not affect the hyperpolarizing shift of the I_{Ca} activation ($V_{0.5,act}$: $Ca_V1.3_{42A} + CaM_{1234}$: −16.3 ± 0.5 mV, $n = 8$) suggesting that the shift in activation voltage occurs independent of CaM as also shown previously for $Ca_V1.4$ (15). Taken together, these data provide unequivocal evidence that the CTM in $Ca_V1.3$ channels not only modulates its activity range but also moderates CDI.

$Ca_V1.3$ CTM Lies within the Most Distal C-terminal Domain Highly Conserved in LTCCs—To further strengthen this hypothesis and pinpoint important structural domains, we tested if different C-terminal truncations exhibit similar gating effects. In accordance to the C-terminal peptide C_{122} important for $Ca_V1.4$ channel modulation (15), we deleted the corresponding distal 158 amino acids of $Ca_V1.3_{42}$. The resulting $Ca_V1.3_{\Delta C158}$ channels exhibited I_{Ca} and I_{Ba} activation properties comparable with $Ca_V1.3_{42A}$ (Tables 1 and 2). For I_{Ca}, k_{act} significantly decreased ($Ca_V1.3_{\Delta C158}$: −7.4 ± 0.2, $n = 9$; $p < 0.001$; Table 1), and $V_{0.5,act}$ ($Ca_V1.3_{\Delta C158}$: −14.3 ± 0.4 mV, $n = 9$, $p < 0.001$; Table 1) shifted to more hyperpolarized voltages. Like in $Ca_V1.3_{42A}$, I_{Ca} inactivation was faster, and CDI was more pronounced, and I_{Ba} was slowed (for all data and statistics see Tables 1–3).

To prove the modulatory role of the last 158 amino acid residues, we tested the capability of this C-terminal fragment to restore the gating changes induced by the truncation. Therefore, GFP-fused peptide (GFP-C_{158}) was expressed together with the respective truncated channel. GFP-C_{158} reverted the gating changes observed in $Ca_V1.3_{\Delta C158}$ channels to values sim-

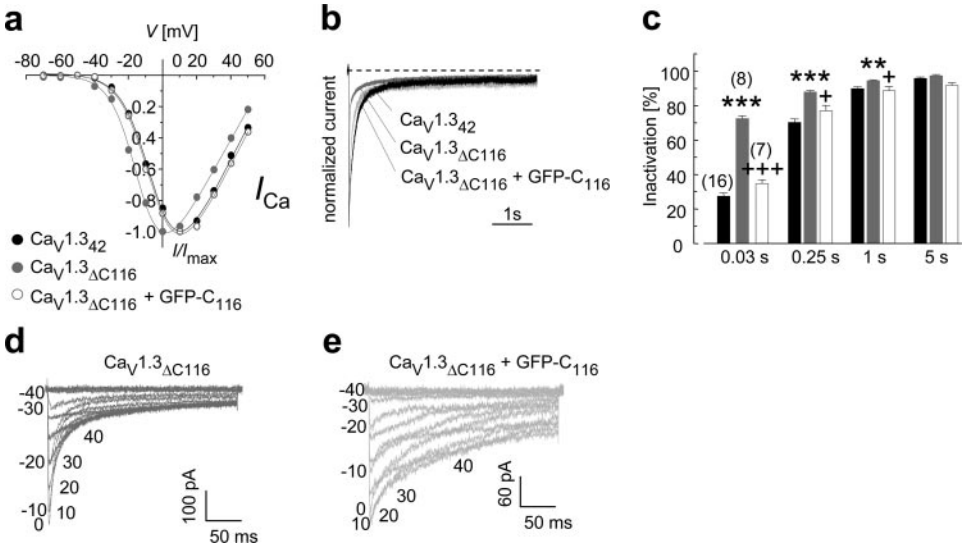

FIGURE 4. **Gating properties of $Ca_V1.3_{\Delta C116}$ channels and effect of the distal CTM peptide C_{116}.** Data for $Ca_V1.3_{42}$ were taken from Fig. 2. *a,* representative normalized *I-V* curves for I_{Ca}. Activation parameters were as follows (in mV): $Ca_V1.3_{42}$: $V_{0.5,act}$, −4.2, and k_{act}, −8.6; $Ca_V1.3_{\Delta C116}$: $V_{0.5,act}$: −12.8, and k_{act}, −7.7; $Ca_V1.3_{\Delta C116}$+GFP-C_{116}: $V_{0.5,act}$, −4.7, and k_{act}, −8.8; Cells: 196l_23, 27g_57, and 27g_91, respectively. *b,* representative current traces of I_{Ca} evoked by a depolarization to V_{max}. Cells: $Ca_V1.3_{\Delta C116}$, 27g_27; $Ca_V1.3_{\Delta C116}$+GFP-C_{116}, 197f_26. *c,* percent I_{Ca} inactivation during test pulses to V_{max}: **, $p < 0.01$; ***, $p < 0.001$, compared with $Ca_V1.3_{42}$ (*black*); +, $p < 0.05$; +++, $p < 0.001$, comparison of $Ca_V1.3_{\Delta C116}$ + GFP-C_{116} (*white*) with $Ca_V1.3_{\Delta C116}$ (*gray*) alone (one-way ANOVA followed by Bonferroni post-test). Number of experiments is given in *parentheses. Error bars* reflect S.E. *d* and *e,* representative I_{Ca} traces for $Ca_V1.3_{\Delta C116}$ (*d*) and $Ca_V1.3_{\Delta C116}$+GFP-C_{116} (*e*). Cells: 27g_67 and 27g_91, respectively. For comparison to $Ca_V1.3_{42}$ see Fig. 2.

ilar to $Ca_V1.3_{42}$; the hyperpolarizing shift of the I_{Ca} activation curve was reversed ($V_{0.5,\ act}$: $Ca_V1.3_{\Delta C158}$ + GFP-C_{158}, −0.8 ± 1.4 mV $n = 8$, $p = 0.3$ *versus* $Ca_V1.3_{42}$; see Table 1); I_{Ca} inactivation was slowed (during 30 ms: $Ca_V1.3_{\Delta C158}$ + GFP-C_{158}; 23.5 ± 1.9%, $n = 8$, $p = 0.2$ *versus* $Ca_V1.3_{42}$; see Table 3), and CDI was less pronounced as indicated by the decrease of the *f* value (at 10 mV, $Ca_V1.3_{\Delta C158}$ + GFP-C_{158}, 0.2 ± 0.08, $n = 6–8$; see Table 3). Peptide-induced reversal of activation and inactivation parameters was also observed in I_{Ba} (Table 2).

To further restrict the protein domain important for CTM activity, we introduced additional truncations in the distal C terminus (Figs. 4–6). Deletion of the last 76 ($Ca_V1.3_{\Delta C76}$) amino acids induced the same gating effects as described for $Ca_V1.3_{\Delta C158}$. However, $Ca_V1.3_{\Delta C76}$ channel activity was not reverted to $Ca_V1.3_{42}$-like behavior by co-expression of peptide GFP-C_{76} (for data and statistics see Tables 1–3). This could not be explained by a lack of GFP-C_{76} expression because full-length expression of this peptide was confirmed in Western blot experiments where the peptide expressed at comparable levels to GFP-C_{158} ($n = 3$, not illustrated). Our data therefore suggest that the last 76 amino acids are required for the formation of CTM activity but cannot functionally recombine with its truncated counterpart to form a modulatory structure. Sequence alignment with other LTCCs (Fig. 6) revealed that truncation ΔC76 cuts in half the most distal highly conserved domain. This may prevent recombination to a functional domain upon co-expression. Hence, we generated $Ca_V1.3_{\Delta C116}$ in which the conserved region was fully removed and subsequently co-expressed as a single peptide. As shown in Fig. 4 and Tables 1–3, $Ca_V1.3_{\Delta C116}$ again exhibited functional I_{Ca} and I_{Ba} properties similar to $Ca_V1.3_{42A}$. However, unlike in $Ca_V1.3_{\Delta C76}$, the gating properties were reversed to those of $Ca_V1.3_{42}$ after co-expression of the GFP-C_{116} peptide (Fig. 4 and Tables 1–3). Co-expression of the corresponding distal peptides not only reversed activation parameters and CDI but also significantly decreased mean I_{Ca} density by 53–63% ($p < 0.05$, $n = 7–11$). A similar trend was also seen for I_{Ba} (41−67%, $n = 7–11$). These data implicate that $Ca_V1.3$ α1 subunits contain critical structural elements required for CTM function within the last 76 amino acids and that the last 116 residues perform CTM activity when co-expressed in HEK-293 cells.

Intramolecular Protein-Protein Interaction Regulates $Ca_V1.3$ Channel Gating—We (15) and others (16) showed that in $Ca_V1.4$ α1 subunits the distal CTM interacts with a more proximal domain containing the EF-hand, pre-IQ-, and IQ-motif. If such a mechanism also holds true for $Ca_V1.3$ channels, CTM-containing peptides should also modulate $Ca_V1.3_{42A}$ (containing EF-PreIQ-IQ). Interestingly, co-expression of GFP-C_{158} neither reversed the $Ca_V1.3_{42A}$-induced hyperpolarizing shift of the activation range of I_{Ca} ($Ca_V1.3_{42A}$ + GFP-C_{158}: $V_{0.5,act}$ = −12.6 ± 1.5 mV, $n = 7$; $p < 0.001$; see Fig. 5*a* and Table 1) and I_{Ba} (Table 2) nor the voltage-dependent inactivation and CDI (Fig. 5, *b* and *c*; Table 3). This prompted us to extend the $Ca_V1.3$ α1 subunit C terminus to residue 1664 thereby including a highly conserved domain downstream of the IQ-motif that is missing in $Ca_V1.3_{42A}$ and also contains the so-called PCRD domain previously identified as binding partner for C-terminal peptides in $Ca_V1.2$ channels (Fig. 6) (17). As expected, the resulting $Ca_V1.3_{\Delta C473}$ channels showed $Ca_V1.3_{42A}$-like gating (Tables 1–3) but, in contrast to $Ca_V1.3_{42A}$, co-expression of GFP-C_{116} restored CDI (Fig. 5, *h* and *i*; Table 3) and the activation and inactivation parameters for I_{Ca} (Fig. 5, *d–f* and *h* and *i*; and Tables 1 and 3) and I_{Ba} (Tables 2 and 3) close to $Ca_V1.3_{42}$ values. These data provide functional evidence for an important role of proximal residues 1626–1664 and the distal 116 amino acids for CTM function.

To provide further evidence for this mechanism, we measured FRET between different YFP-labeled C-terminal fragments and CFP-labeled C_{158} (CFP-C_{158}) as well as CFP-labeled C_{116} (CFP-C_{116}) (Fig. 7). The construct corresponding to the C-terminal fragment of $Ca_V1.3_{42A}$ (YFP-EF-PreIQ-IQ) did not show significant FRET with the CFP-C_{158} probe (legend to Fig. 7). By extending the $Ca_V1.3$ YFP-EF-preIQ-IQ bait to residue 1664 yielding YFP-EF-preIQ-IQ-PCRD, a strong and significant FRET signal was measured with CFP-C_{158} as well CFP-C_{116} (Fig. 7), which is in excellent agreement with our electrophysiological data. Accordingly, no FRET was observed when CFP-C_{76} peptide was used as a probe (not shown). For $Ca_V1.2$

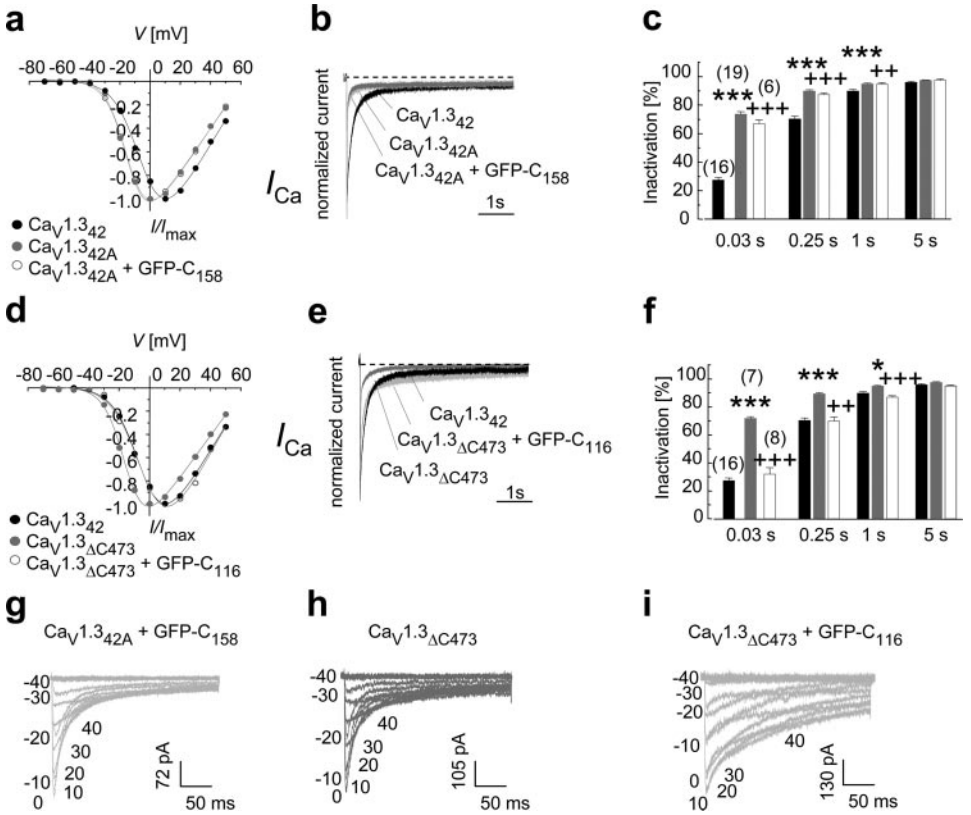

FIGURE 5. **$Ca_V1.3_{\Delta C473}$ channel properties in absence and presence of distal CTM peptide C_{116}.** Data for $Ca_V1.3_{42}$ (*black*) and $Ca_V1.3_{42A}$ (*gray*) were taken from Figs. 2 and 4. *a,* representative normalized *I-V* curves for I_{Ca}. Activation parameters (in mV): $Ca_V1.3_{42A}$: $V_{0.5,act}$, −14.3, and k_{act}, −6.8; $Ca_V1.3_{42A}$ + GFP-C_{158}: $V_{0.5,act}$, −13.5 and k_{act}, −7.2; Cells: 196l_32 and 217c_3, respectively. *b,* representative current traces of I_{Ca} evoked a 10-s depolarization to V_{max}. Cells: $Ca_V1.3_{42A}$ + GFP-C_{158}, 227k_19; $Ca_V1.3_{42}$, 316h_51; $Ca_V1.3_{42A}$, 187g_46. *c,* percent I_{Ca} inactivation during test pulses to V_{max}: *, $p < 0.05$; ***, $p < 0.001$ compared with $Ca_V1.3_{42}$; ++, $p < 0.01$; +++, $p < 0.001$, comparison of $Ca_V1.3_{42A}$ + GFP-C_{158} with $Ca_V1.3_{42A}$ alone. *d,* representative normalized *I-V* curves for I_{Ca}. Activation parameters (in mV): $Ca_V1.3_{\Delta C473}$: $V_{0.5,act}$, −14.4, and k_{act}, −7.1; $Ca_V1.3_{\Delta C473}$ +GFP-C_{116}: $V_{0.5,act}$, −2.4, and k_{act}, −9.4; Cells: 177i_1 and 167j_24, respectively. *e,* same conditions as in *b*. Cells: $Ca_V1.3_{\Delta C473}$, 247h_25; $Ca_V1.3_{\Delta C473}$ +GFP-C_{116}, 167j_14. *f,* percent I_{Ca} inactivation during test pulses to V_{max}: *, $p < 0.05$; **, $p < 0.01$; ***, $p < 0.001$ compared with $Ca_V1.3_{42}$; +, $p < 0.05$; ++, $p < 0.01$; +++, $p < 0.001$, comparison of $Ca_V1.3_{\Delta C473}$ + GFP-C_{116} with $Ca_V1.3_{\Delta C473}$ alone. *g–i,* representative I_{Ca} traces for $Ca_V1.3_{42A}$ + GFP-C_{158} (*g*), $Ca_V1.3_{\Delta C473}$ (*h*), and $Ca_V1.3_{\Delta C473}$ + GFP-C_{116} (*i*) correspond to *I-V* curves in *a* and *d*. For comparison to $Ca_V1.3_{42}$ and $Ca_V1.3_{42A}$ see Fig. 2. For statistics: in *a* and *d,* Student's *t* test; *c* and *f,* one-way ANOVA followed by Bonferroni post-test. Number of experiments is given in *parentheses*. *Error bars* reflect S.E.

channels, interaction between a pair of arginine residues in the PCRD and a set of negatively charged residues in the distal C-terminal region (DCRD) was predicted (Fig. 6) (17). As shown in Fig. 7, mutating the two conserved arginines in the $Ca_V1.3$ PCRD to glutamine (EF-preIQ-IQ-PCRD^{RRQQ} containing R1640Q and R1641Q) still supported a significant FRET signal when co-expressed with CFP-C_{116}. Using probe CFP-C_{116}^{DEQQ}, where the two negative charges in DCRD conserved in $Ca_V1.3$ were neutralized (D2073Q and E2076Q), significant FRET was eliminated for both EF-preIQ-IQ-PCRD and EF-preIQ-IQ-PCRD^{RRQQ}. Therefore, neutralization of the two positive charges of the PCRD arginines is not sufficient to prevent the binding interaction suggesting that other binding determinants exist in the conserved domain between residues 1626 and 1664. Our data indicate an essential role of the two negative charges in the $Ca_V1.3_{42}$ DCRD region, similar to $Ca_V1.2$.

To address the question if the moderation of CDI by the CTM involves modulation of CaM interaction with its C-terminal interaction domains, we measured if the presence of the CTM can affect the constitutive binding of CaM at resting intracellular Ca^{2+} concentrations. We measured FRET between CFP-labeled calmodulin (CFP-CaM) and the fragments YFP-EF-preIQ-IQ (mimicking the short $Ca_V1.3_{42A}$), YFP-EF-preIQ-IQ-PCRD, and a peptide corresponding to the complete $Ca_V1.3$ C terminus (YFP-$Ca_V1.3$-C terminus), including the CTM (corresponding to the long $Ca_V1.3_{42}$). Whereas significant N_{FRET} ($p < 0.001$ *versus* YFP-$Ca_V1.3$-C terminus; one-way ANOVA, Bonferroni post-test) was measured for YFP-EF-preIQ-IQ (0.185 ± 0.009, $n = 12$) and YFP-EF-preIQ-IQ-PCRD (0.235 ± 0.007, $n = 3$), no significant N_{FRET} was obtained for YFP-$Ca_V1.3$-C terminus (0.039 ± 0.017, $n = 6$, $p = 0.07$. one-sample *t* test, compared with 0). This is in excellent agreement with our previous findings in $Ca_V1.4$ channels (15) indicating that the $Ca_V1.3$ CTM interferes with CaM coordination to the C terminus in intact cells. This also provides a plausible mechanism for explaining the moderation of CDI.

We also investigated whether the function of the CTM was prevented by alternative splicing of exon 44 in the post-IQ region of the C terminus (Fig. 6). Introduction of 9 amino acid corresponding to exon 44 into a full-length $Ca_V1.3$ construct ($Ca_V1.3_{42+44}$) exhibited activation parameters similar to $Ca_V1.3_{42}$ (I_{Ba}: $V_{0.5,\,act} = -14.8 \pm 1.2$ mV, $k_{act} = -9.3 \pm 0.3$ mV, $n = 14$; I_{Ca}, $V_{0.5,\,act} = -3.7 \pm 1.02$ mV, $k_{act} = -10.6 \pm 0.3$ mV, $n = 8$) suggesting that CTM function was not prevented by alternative splicing of this exon.

$Ca_V1.3_{42}$ and $Ca_V1.3_{42A}$ Are Both Expressed in Mouse and Human Tissues—We employed PCR to determine whether both long (CTM-containing) and short (CTM-deficient) splice variants are expressed in mouse and human tissue. RT-PCR experiments identified both exon 42 and 42A mRNA in different mouse brain regions and the organ of Corti (Fig. 8*a*) as well as in human brain, heart, retina, and pancreas (Fig. 8*b*). Using quantitative real time PCR, we determined the relative abundance of these transcripts in mouse whole-brain as well as several brain sub-regions (Fig. 8*c*). Because exons 42 and 42A are used in a mutually exclusive manner, we calculated the relative amount of exon 42A as percentage of the sum of exon 42 and 42A containing mRNA molecules in samples from two to three independent RNA preparations. Although exon 42 was the predominant form in whole-brain and all sub-regions investigated,

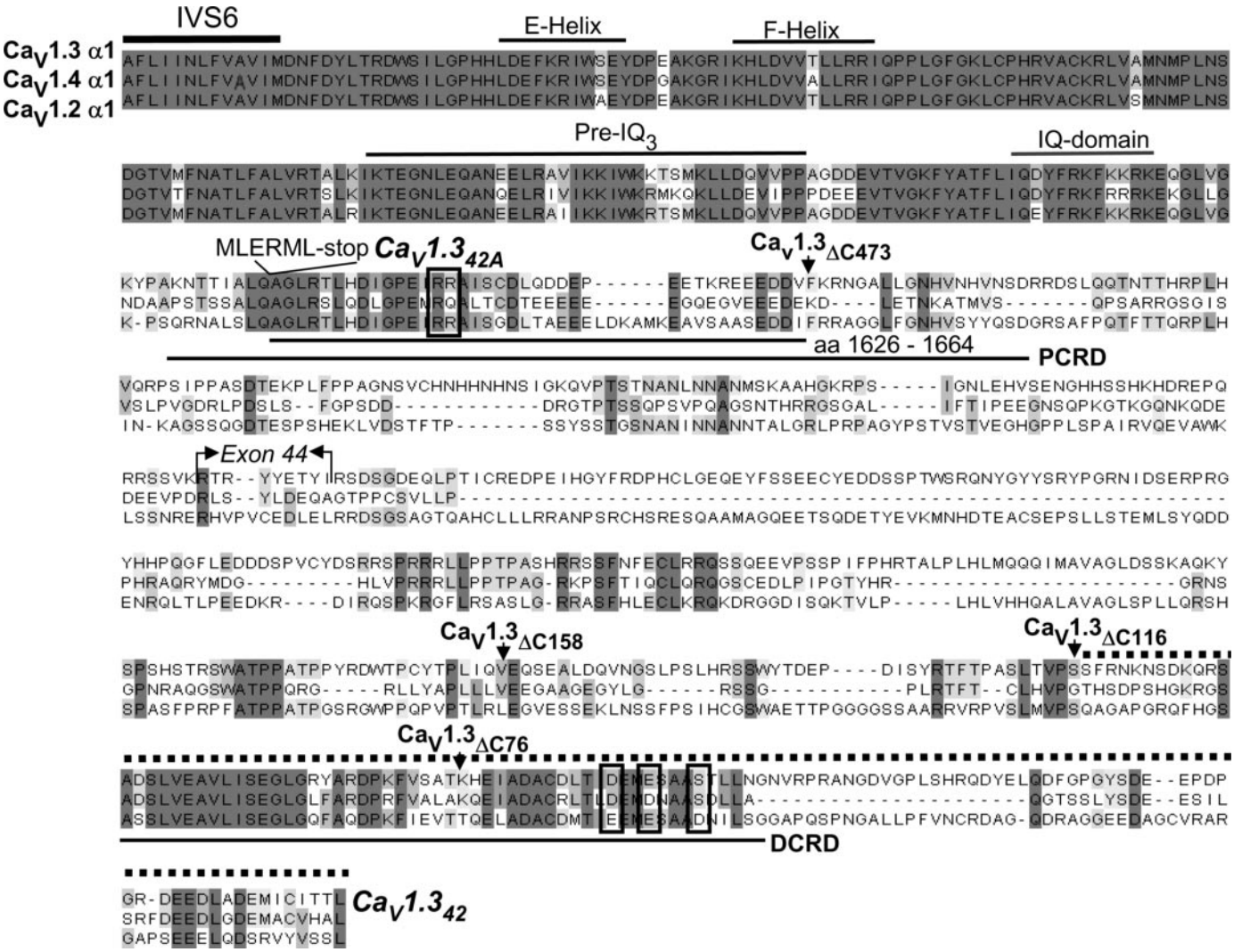

FIGURE 6. **Sequence alignment of LTCC C termini.** A sequence alignment of neuronal human $Ca_V1.3$ (GenBank™ accession number NM_000720), $Ca_V1.4$ (GenBank™ accession number AJ224874), and $Ca_V1.2$ (uniprot accession number Q13936) $\alpha1$ subunits is shown. Sequence identity (*dark gray*), similarity (*light gray*) and gaps (−) are indicated. *PCRD*, proximal C-terminal regulatory domain; *DCRD*, distal C-terminal regulatory domain; CTM, *dotted line*. Position of $Ca_V1.3_{42A}$ and truncation mutants $Ca_V1.3_{\Delta C473}$, $Ca_V1.3_{\Delta C158}$, $Ca_V1.3_{\Delta C116}$, and $Ca_V1.3_{\Delta C76}$ are indicated by *black arrows*. Position of exon 44 is given.

significant expression of exon 42A was also found. In whole-brain preparations, exon 42A was 11.0 ± 0.6% ($n = 8$) of the two mRNAs. Variable expression was found in brain sub-regions with the highest expression in cerebellum (17.1 ± 2.5%, $n = 4$) and the nucleus accumbens (13.3 ± 1.5%, $n = 3$) and the lowest in olfactory bulb (2.1 ± 0.2%, $n = 3$). These data suggest that the short $Ca_V1.3$ splice variant can contribute significantly to overall $Ca_V1.3$ activity. Notably, our experiments do not rule out the possibility of other short isoforms with gating properties similar to $Ca_V1.3_{42A}$. Therefore the contribution of short forms to overall $Ca_V1.3$ expression is likely to be underestimated by our experiments.

DISCUSSION

Here we present functional evidence for a C-terminal automodulatory domain that controls voltage- and Ca^{2+}-dependent gating properties of $Ca_V1.3$ LTCCs. Such modulation has not been described for $Ca_V1.3$ channels before. The absence of the CTM in the short splice variant $Ca_V1.3_{42A}$ provides functional diversity to $Ca_V1.3$ channels. $Ca_V1.3_{42A}$ mRNA is expressed together with $Ca_V1.3_{42}$ in different mouse and human tissues suggesting that this functional diversity is of physiological relevance to adapt $Ca_V1.3$ channel activity for specific physiological needs. Activation at negative voltages is one hallmark of $Ca_V1.3$ channels (for review see Ref. 6) crucial for adequate neurotransmitter release in IHCs and pacemaker function in the SAN, atrioventricular conduction (30, 31), and neuronal excitability (7, 32). In the absence of the CTM, $V_{0.5,act}$ is shifted about 10 mV to more negative voltages by decreasing the slope factor of the activation curve but without measurable effects on the activation threshold. This effect was not correlated with current densities, was independent from cell passage number, and was reproducibly observed for splice variant $Ca_V1.3_{42A}$ as well as for several truncations mutants. Moreover, it could not be attributed to artificial manipulations of the $Ca_V1.3\alpha1$ subunits because it was observed in wild-type channel constructs not modified by fusion to GFP or introduction of

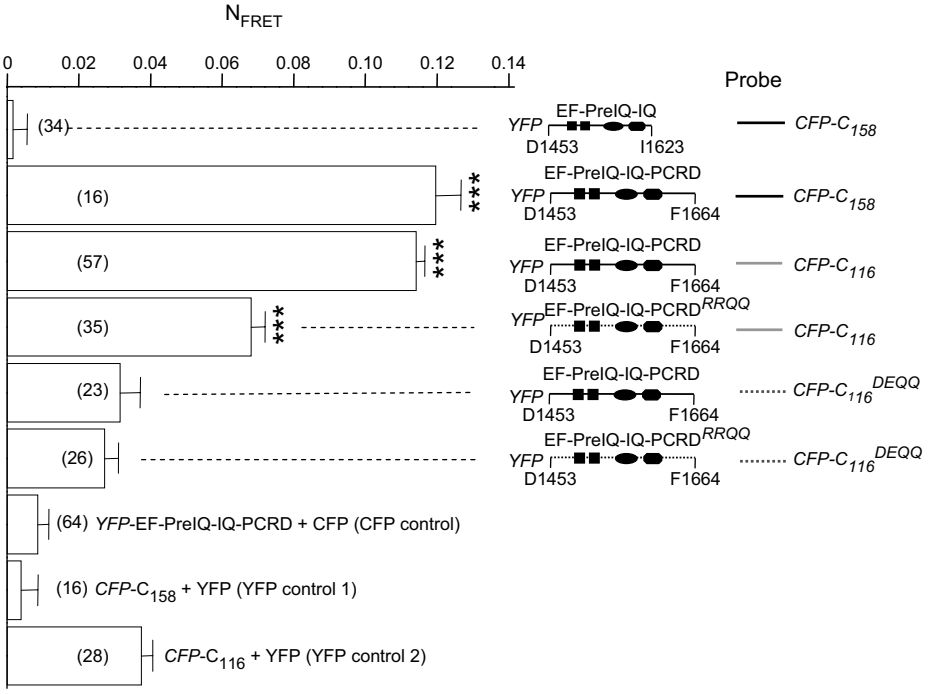

FIGURE 7. **FRET analysis of the binding of peptide C_{158} or C_{116} to various fragments of the $Ca_V1.3$ C terminus.** N_{FRET} values obtained from co-expression of CFP-C_{158} or CFP-C_{116} (*probe*) with the indicated YFP-tagged $Ca_V1.3$ C-terminal fragments in HEK-293 cells. All constructs showed a homogeneous intracellular distribution. As controls, N_{FRET} values are given for CFP co-expressed with YFP-EF-PreIQ-IQ-PCRD (*CFP control*) and YFP with probes CFP-C_{158} (*YFP control 1*) and CFP-C_{116} (*YFP control 2*). Controls are not significantly different from zero (one-sample *t* test against 0). Interaction between fragments was considered when significant difference to both the CFP- and the corresponding YFP control was observed (***, $p < 0.001$, one-way ANOVA followed by Bonferroni post-test).

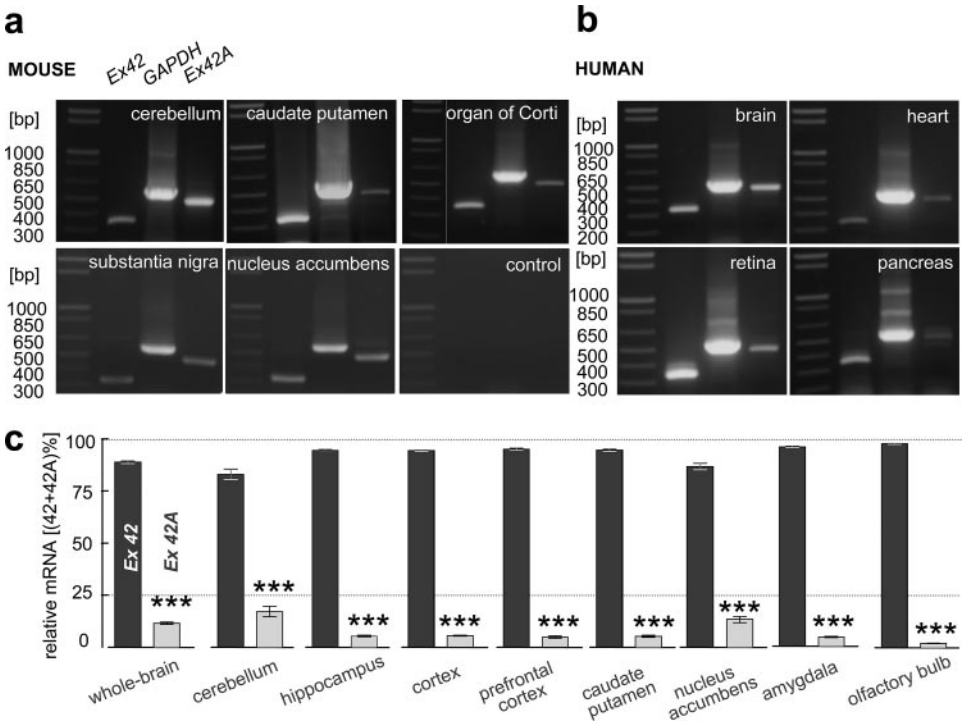

FIGURE 8. **Tissue expression of $Ca_V1.3$ C-terminal splice variants.** Qualitative RT-PCR experiments showing expression of both long (containing exon (*Ex*) 42) and short (containing exon 42A) $Ca_V1.3$ isoforms in different mouse (*a*) and human (*b*) tissues. GAPDH was used as a housekeeping gene. One representative out of at least three independent experiments is shown. Quantitative Taqman RT-PCR experiments in *a* (*right*), show the relative expression of exons 42 and 42A in percent of total signal in mouse whole-brain and several brain subregions (***, $p < 0.001$, unpaired Students *t* test, all significantly different from 0, one sample *t* test). Data are given as means ± S.E.

other tags. In addition, co-expression of peptides containing the CTM with truncation mutants $Ca_V1.3_{\Delta C116}$, $Ca_V1.3_{\Delta C158}$, and $Ca_V1.3_{\Delta C473}$ reversed this shift. Cells may therefore adjust the activity of $Ca_V1.3$-mediated signaling by varying the relative abundance of CTM-containing splice variants.

The functional properties of $Ca_V1.3_{42}$ and $Ca_V1.3_{42A}$ channels have been studied in previous reports. In two studies functional differences were observed between these splice variants, termed $Ca_V1.3a$ and $Ca_V1.3b$ therein, respectively. Calin-Jageman *et al.* (39) found that VDF of rat $Ca_V1.3$ channels expressed in HEK-293T cells was significantly more pronounced for $Ca_V1.3_{42A}$ than for $Ca_V1.3_{42}$ suggesting an autoinhibitory effect of the C-terminal tail on VDF. Comparisons of *I-V* relationship and I_{Ca} were not reported in this study. Zhang *et al.* (37) expressed hemagglutinin-tagged splice variants in *Xenopus laevis* oocytes and found that I_{Ba} of the $Ca_V1.3_{42A}$ construct was not only larger in amplitude but also its *I-V* relationship was shifted toward more negative voltages, similar to our findings. I_{Ca} was not reported. Although a more detailed comparison of the biophysical properties of $Ca_V1.3_{42}$ and $Ca_V1.3_{42A}$ was not the purpose of these studies, they support a modulatory role of the C terminus. In contrast, other groups using the corresponding (5, 13) or different (33) rat $Ca_V1.3_{42}$ and $Ca_V1.3_{42A}$ $\alpha 1$ subunit analogues found neither major differences in the activation voltage range nor in CDI (13). Therefore, $V_{0.5,act}$ and V_{max} values for I_{Ba} as well as the extent of CDI closely resemble our human $Ca_V1.3_{42A}$ channels (5, 13, 12). Even though at present the molecular basis for this difference is unclear, chimeric constructs between rat and human $Ca_V1.3$ constructs expressed under identical experimental conditions (*e.g.* to exclude confounding effects of the heterologous expression system

and/or accessory subunit composition) will help to clarify this question.

Our observation of a modulatory C-terminal domain in $Ca_V1.3$ adds to recent discoveries of a similar regulatory principle in other LTCC isoforms (see Refs. 15, 17, and references therein). Autoinhibitory control of $Ca_V1.2$ channel function was proposed to be based on a binding interaction between a pair of exposed arginine residues and negatively charged residues in α-helical motifs in a proximal (PCRD) and a distal (DCRD) conserved region of the C terminus, respectively (17). In our human $Ca_V1.3$ channels, 39 residues (1626–1664) comprising the proximal conserved domain containing the PCRD were necessary to confer modulation, as well as FRET to co-expressed CTM-containing peptides. Neutralization of the two conserved positive charges in PCRD did not prevent FRET implying other essential motifs within this 39-residue PCRD domain. Evidence for a role of DCRD comes from the finding that two conserved negative charges are required to support binding of CFP-C_{116} to the upstream domain.

The functional consequences of LTCC C-terminal modulation appear different in $Ca_V1.2$ and $Ca_V1.3$ channels. In $Ca_V1.2$, C-terminal truncation does not induce a more negative $V_{0.5,act}$, but overexpression of the distal C terminus shifts the activation range to more positive voltages and reduces the coupling efficiency of voltage-sensing to channel opening (17). This is in contrast to $Ca_V1.4$ and $Ca_V1.3$ channels in which removal of the CTM facilitates activation within a more negative voltage range and CTM co-expression restores gating (15 and this paper). Differences between LTCCs also exist with respect to the moderation of CDI. Although in both channels the CTM is able to interfere with CaM association, the CTM completely prevents CDI in $Ca_V1.4$ (15) but only moderates CDI in $Ca_V1.3$. To our knowledge the effects of the C-terminal autoinhibitory domain on CDI of $Ca_V1.2$ channels has not been systematically analyzed so far.

Our finding of C-terminal modulation of $Ca_V1.3$ also raises the important question about potential post-translational proteolytic cleavage in the long C terminus. Such has been reported for $Ca_V1.1$ and $Ca_V1.2$ channels (18, 34). The $Ca_V1.2$ cleavage product not only serves as a potent autoinhibitor when it remains noncovalently bound to the channel (17) but may also dissociate from the $\alpha1$ subunit thereby serving as a transcriptional regulator after translocation to the nucleus (19). So far biochemical evidence for $Ca_V1.3$ C-terminal cleavage is lacking, and it does not appear to function as a transcriptional regulator (19). Instead, as demonstrated here, alternative splicing can generate short and functionally distinct $Ca_V1.3$ variants. Such splicing has not yet been reported for $Ca_V1.1$, $Ca_V1.2$, or $Ca_V1.4$ channels.

Our data predict that the expression of $Ca_V1.3_{42A}$ would allow a cell to promote Ca^{2+} entry through $Ca_V1.3$ channels at sub-threshold voltages as predicted from the negative shift of the window current (Fig. 2*e*). Stronger activation at more negative voltages may also facilitate the onset of upstate potentials in neurons. However, during maintained depolarization, the faster CDI would limit Ca^{2+} entry through these channels as relevant in neurons with $Ca_V1.3$-dependent pacemaking, *e.g.* dopamine-containing neurons in the substantia nigra (36). Whereas negative activation of an even small $Ca_V1.3$ current could trigger pacemaking, faster CDI would limit Ca^{2+} entry during ensuing action potentials. This may be important in these neurons that are susceptible to Ca^{2+} toxicity and neurodegeneration in Parkinson disease (36). In contrast, the CTM in $Ca_V1.3_{42}$ channels may be required for longer lasting Ca^{2+} signals triggered by stronger depolarization inducing cAMP-response element-binding protein phosphorylation and synaptic plasticity (37).

Our study raises several important questions that need to be addressed in future studies. The fact that the increase in current density observed in $Ca_V1.3_{42A}$ channels seems not to be due to increased expression density (and increased gating currents, see Fig. 2) suggests differences in the unitary current (*e.g.* increase in single-channel conductance or open probability or prolonged open times). Single-channel analysis will also be required to provide a mechanistic explanation for the shift in activation gating parameters in the short $Ca_V1.3$ channels. Changes in the unitary conductance of $Ca_V1.2$ channels induced by structural alterations within the CaM interaction domains in the C terminus well outside the known pore-forming regions have been described (38) providing evidence for a conformational link of the CaM binding domain not only with the gating machinery but also with the channel pore.

Several proteins binding to interaction domains of the C terminus have been described. For example, in neurons the multifunctional PDZ protein Erbin binds to a PDZ-binding domain formed by the last four amino acid residues of $Ca_V1.3_{42}$ and thereby relieves the autoinhibitory effect of the C terminus on VDF (see Ref. 39 and see above). Also Shank protein (40) and RIM-binding protein (41) are predicted to bind selectively to the C terminus of $Ca_V1.3$ channels and may therefore affect CTM function. The fact that the distal C terminus comprising the CTM also contains regulatory sites, including sites for cAMP-dependent protein kinase phosphorylation (42) and AKAP-15 (43), raises the interesting possibility that their interference with the activity of the CTM itself could also serve as mechanism to fine-tune $Ca_V1.3$ function. Such a mechanism has recently been proposed to explain the still enigmatic mechanism of cAMP-dependent protein kinase-dependent activation of $Ca_V1.2$ LTCCs (35).

Taken together, we have identified a modulatory domain in $Ca_V1.3$ LTCCs responsible for profound differences in the Ca^{2+}- and voltage-dependent gating of the different C-terminal splice variants. Given that many unique physiological functions of $Ca_V1.3$ depend on the negative activation range of the channel and the amount of Ca^{2+} ions entering during plateau (7) or single action potentials (8), our findings identify the CTM and factors that modify its activity (such as alternative splicing) as elements suitable to determine electrical excitability. Future experiments must also address the interesting possibility that interference with this C-terminal regulatory mechanism can also be exploited for pharmacological intervention, as an alternative to classical Ca^{2+} channel modulators.

Acknowledgments—We thank Dr. Simone Sartori for the preparation of mouse brain subregions. We thank Ursula Einzinger, Perrine Busquet, and Gilda Pelster for help with quantitative RT-PCRs. We also thank Sylvia Kaperek for preparation of cDNA from the mouse organ of Corti, Gilda Pelster and Irene Frischauf, Heike Kahr, and Sabine Buchegger for excellent technical assistance.

REFERENCES

1. Catterall, W. A., Perez-Reyes, E., Snutch, T. P., and Striessnig, J. (2005) *Pharmacol. Rev.* **57,** 411–425
2. Striessnig, J. (2007) *J. Physiol.* (*Lond.*) **585,** 643–644
3. Platzer, J., Engel, J., Schrott-Fischer, A., Stephan, K., Bova, S., Chen, H., Zheng, H., and Striessnig, J. (2000) *Cell* **102,** 89–97
4. Koschak, A., Reimer, D., Huber, I., Grabner, M., Glossmann, H., Engel, J., and Striessnig, J. (2001) *J. Biol. Chem.* **276,** 22100–22106
5. Xu, W., and Lipscombe, D. (2001) *J. Neurosci.* **21,** 5944–5951
6. Lipscombe, D., Helton, T. D., and Xu, W. (2004) *J. Neurophysiol.* **92,** 2633–2641
7. Olson, P. A., Tkatch, T., Hernandez-Lopez, S., Ulrich, S., Ilijic, E., Mugnaini, E., Zhang, H., Bezprozvanny, I., and Surmeier, D. J. (2005) *J. Neurosci.* **25,** 1050–1062
8. Helton, T. D., Xu, W., and Lipscombe, D. (2005) *J. Neurosci.* **25,** 10247–10251
9. Halling, D. B., Aracena-Parks, P., and Hamilton, S. L. (2006) *Sci. STKE 2006*, er1
10. Liang, H., DeMaria, C. D., Erickson, M. G., Mori, M. X., Alseikhan, B. A., and Yue, D. T. (2003) *Neuron* **39,** 951–960
11. Soldatov, N. M., Zuhlke, R. D., Bouron, A., and Reuter, H. (1997) *J. Biol. Chem.* **272,** 3560–3566
12. Shen, Y., Yu, D., Hiel, H., Liao, P., Yue, D. T., Fuchs, P. A., and Soong, T. W. (2006) *J. Neurosci.* **26,** 10690–10699
13. Yang, P. S., Alseikhan, B. A., Hiel, H., Grant, L., Mori, M. X., Yang, W., Fuchs, P. A., and Yue, D. T. (2006) *J. Neurosci.* **26,** 10677–10689
14. Cui, G., Meyer, A. C., Calin-Jageman, I., Neef, J., Haeseleer, F., Moser, T., and Lee, A. (2007) *J. Physiol.* (*Lond.*) **585,** 791–803
15. Singh, A., Hamedinger, D., Hoda, J. C., Gebhart, M., Koschak, A., Romanin, C., and Striessnig, J. (2006) *Nat. Neurosci.* **9,** 1108–1116
16. Wahl-Schott, C., Baumann, L., Cuny, H., Eckert, C., Griessmeier, K., and Biel, M. (2006) *Proc. Natl. Acad. Sci. U. S. A.* **103,** 15657–15662
17. Hulme, J. T., Yarov-Yarovoy, V., Lin, T. W., Scheuer, T., and Catterall, W. A. (2006) *J. Physiol.* (*Lond.*) **576,** 87–102
18. Hulme, J. T., Konoki, K., Lin, T. W., Gritsenko, M. A., Camp, D. G., II, Bigelow, D. J., and Catterall, W. A. (2005) *Proc. Natl. Acad. Sci. U. S. A.* **102,** 5274–5279
19. Gomez-Ospina, N., Tsuruta, F., Barreto-Chang, O., Hu, L., and Dolmetsch, R. (2006) *Cell* **127,** 591–606
20. Ganesan, A. N., Maack, C., Johns, D. C., Sidor, A., and O'Rourke, B. (2006) *Circ. Res.* **98,** e11-8
21. Gao, T., Cuadra, A. E., Ma, H., Bunemann, M., Gerhardstein, B. L., Cheng, T., Eick, R. T., and Hosey, M. M. (2001) *J. Biol. Chem.* **276,** 21089–21097
22. Grabner, M., Dirksen, R. T., and Beam, K. G. (1998) *Proc. Natl. Acad. Sci. U. S. A.* **95,** 1903–1908
23. Michna, M., Knirsch, M., Hoda, J. C., Muenkner, S., Langer, P., Platzer, J., Striessnig, J., and Engel, J. (2003) *J. Physiol.* (*Lond.*) **553,** 747–758
24. Koschak, A., Obermair, G. J., Pivotto, F., Sinnegger-Brauns, M. J., Striessnig, J., and Pietrobon, D. (2007) *J. Neurosci.* **27,** 3855–3863
25. Huber, I., Wappl, E., Herzog, A., Mitterdorfer, J., Glossmann, H., Langer, T., and Striessnig, J. (2000) *Biochem. J.* **347,** 829–836
26. Xia, Z., and Liu, Y. (2001) *Biophys. J.* **81,** 2395–2402
27. Hui, A., Ellinor, P. T., Krizanova, O., Wang, J.-J., Diebold, R. J., and Schwartz, A. (1991) *Neuron* **7,** 35–44
28. Williams, M. E., Feldman, D. H., McCue, A. F., Brenner, R., Velicelebi, G., Ellis, S. B., and Harpold, M. M. (1992) *Neuron* **8,** 71–84
29. Pichler, M., Cassidy, T. N., Reimer, D., Haase, H., Kraus, R., Ostler, D., and Striessnig, J. (1997) *J. Biol. Chem.* **272,** 13877–13882
30. Mangoni, M. E., Couette, B., Bourinet, E., Platzer, J., Reimer, D., Striessnig, J., and Nargeot, J. (2003) *Proc. Natl. Acad. Sci. U. S. A.* **100,** 5543–5548
31. Matthes, J., Yildirim, L., Wietzorrek, G., Reimer, D., Striessnig, J., and Herzig, S. (2004) *Naunyn-Schmiedeberg's Arch. Pharmacol.* **369,** 554–562
32. Bean, B. P. (2007) *Nature* **447,** 1059–1060
33. Safa, P., Boulter, J., and Hales, T. G. (2001) *J. Biol. Chem.* **276,** 38727–38737
34. Hell, J. W., Westenbroek, R. E., Breeze, L. J., Wang, K. K., Chavkin, C., and Catterall, W. A. (1996) *Proc. Natl. Acad. Sci. U. S. A.* **93,** 3362–3367
35. Hulme, J. T., Westenbroek, R. E., Scheuer, T., and Catterall, W. A. (2006) *Proc. Natl. Acad. Sci. U. S. A.* **103,** 16574–16579
36. Chan, C. S., Guzman, J. N., Ilijic, E., Mercer, J. N., Rick, C., Tkatch, T., Meredith, G. E., and Surmeier, D. J. (2007) *Nature* **447,** 1081–1086
37. Zhang, H., Fu, Y., Altier, C., Platzer, J., Surmeier, D. J., and Bezprozvanny, I. (2006) *Eur. J. Neurosci.* **23,** 2297–2310
38. Kepplinger, K. J., Kahr, H., Forstner, G., Sonnleitner, M., Schindler, H., Schmidt, T., Groschner, K., Soldatov, N. M., and Romanin, C. (2000) *FEBS Lett.* **477,** 161–169
39. Calin-Jageman, I., Yu, K., Hall, R. A., Mei, L., and Lee, A. (2007) *J. Neurosci.* **27,** 1374–1385
40. Zhang, H., Maximov, A., Fu, Y., Xu, F., Tang, T. S., Tkatch, T., Surmeier, D. J., and Bezprozvanny, I. (2005) *J. Neurosci.* **25,** 1037–1049
41. Hibino, H., Pironkova, R., Onwumere, O., Vologodskaia, M., Hudspeth, A. J., and Lesage, F. (2002) *Neuron* **34,** 411–423
42. Qu, Y., Baroudi, G., Yue, Y., El-Sherif, N., and Boutjdir, M. (2005) *Am. J. Physiol.* **288,** H2123–H2130
43. Hulme, J. T., Ahn, M., Hauschka, S. D., Scheuer, T., and Catterall, W. A. (2002) *J. Biol. Chem.* **277,** 4079–4087
44. [1] To whom correspondence should be addressed. Tel.: 43-512-507-5602; Fax: 42-512-507-2931; E-mail: alexandra.koschak@uibk.ac.at.